Eur. Phys. J. D **30**, 171–179 (2004)
DOI: 10.1140/epjd/e2004-00085-3

THE EUROPEAN PHYSICAL JOURNAL D

Multiple ionization effects on L X-ray intensity ratios in Hf, Ta, Re, Ir, Pt, Au and Pb due to proton bombardment at energies 1–5 MeV

G.J. Naga Raju, G.A.V. Ramana Murty, B. Seetharami Reddy, T. Seshi Reddy, S. Lakshminarayana, and S. Bhuloka Reddy[a]

Swami Jnanananda Laboratories for Nuclear Research, Andhra University, Visakhapatnam 530 003, India

Received 13 January 2004 / Received in final form 27 March 2004
Published online 6 July 2004 –

Abstract. The L X-ray intensity ratios in the elements Hf, Ta, Re, Ir, Pt, Au and Pb due to proton bombardment at energies from 1 to 5 MeV are measured and compared with the ECPSSR theoretical intensity ratios. The L_α/L_l intensity ratios obtained in the present work are in good agreement with theoretical values while the L_β/L_γ and L_α/L_β intensity ratios are consistently lower than the theoretical values. This deviation may be explained in terms of multiple ionization effects in M, N and O shells.

PACS. 32.80.Hd Auger effect and inner-shell excitation or ionization – 32.30.Rj X-ray spectra – 41.75.-i Charged-particle beams – 41.75.Ak Positive-ion beams

1 Introduction

Measurement of L X-ray intensity ratios with protons is important both for verifying the existing theories and also to refine the analysis of PIXE spectra. PIXE spectrum is very complex having K and L X-ray components of several elements. Due to limitation in the efficiency of low energy Si(Li) detector to detect high energy X-rays, in PIXE spectrum, the elements whose atomic number is smaller than about 50 are identified by the corresponding K X-rays energies while the elements whose atomic number is greater than about 50 are identified by their corresponding energies of L X-ray components. The L X-ray lines of high Z elements overlap with the K X-ray lines of low Z elements. Also, there is a possibility of some of the L X-ray components of a particular element overlapping with the L X-ray components of a nearby element. The overlap of K and L X-ray lines of different elements creates problems in the quantitative estimation of elemental concentrations. Hence for a proper deconvolution of overlapped X-ray lines, the relative intensities of different L X-ray components of high Z elements should be accurately known. Where the experimental L X-ray intensity ratios are not available for any element, appropriate theoretical intensity ratios of that element are used during the process of deconvolution. Since the L X-ray ionization cross-sections are energy dependent, the intensity ratios are also energy dependent. In order to have larger data base of L X-ray intensity ratios at different projectile energies and to check the validity of different theories which support the experimental results, there is a need to carry out the measurement of L X-ray intensity ratios in some high Z elements at different proton energies.

The theoretical L X-ray intensity ratios are obtained from the production cross-sections of the corresponding X-ray components. These production cross-sections are estimated theoretically from the theoretical ionization cross-sections. The validity of theoretical L X-ray intensity ratios thus depends on the validity of theoretical ionization cross-sections and different databases of fluorescent yields and C-K yield vales that are used.

Inner shell ionization is a sum of direct ionization to the target's continuum and electron capture from the target atom by the projectile to its unoccupied states. The direct ionization of a target electron to the continuum is the principal mechanism of ionization for $Z_1 \ll Z_2$ and $v_1 \gg v_{2L}$ where Z_1 and Z_2 refer to the atomic numbers of the projectile and the target atom respectively and v_1 and v_{2L} represent the velocities of the projectile and target electron.

For asymmetric ion-atom collisions ($Z_1/Z_2 \ll 1$), the Direct Ionization is the dominating process and is treated by several theoretical approaches such as Plane Wave Born Approximation (PWBA) [1–3], Semi Classical Approximation (SCA) [4,5] and Binary Encounter Approximation (BEA) [6]. These first order theories can explain the K shell ionization cross-sections for any of the projectile-target combinations. These theories did not explain the

[a] e-mail: sbr_r@yahoo.com

L sub shell ionization cross-sections even for low projectiles such as protons or helium ions. The ECPSSR theory [7,8] goes beyond the first order theories by accounting for the energy loss (E) of the projectile in the process of ionization, the coulomb deflection (C) of the projectile in the vicinity of the target nucleus, the perturbation of the inner shell electrons of the target atom by the projectile in terms of the perturbed stationary states (PSS) and the relativistic description of the inner shell electrons.

From the compilation of Paul and co-workers [9,10], a great amount of understanding has been achieved in explaining the experimental data on K shell ionization cross-sections. From the compilations of Sokhi and Crompton [11] and recently by Orlic et al. [12], significant discrepancies are noticed between experimental and theoretical L shell cross-sections. It is also observed by some authors [13–19] that the relative L X-ray intensities in some high Z elements due to protons are deviate from ECPSSR theory, particularly at low projectile energies. Lapicki [20] pointed out that there is no unique theory, which explain the experimental L sub shell ionization data even by the lightest ions-protons at low energies. These discrepancies led to the modification of ECPSSR theory by introducing various corrections for the description of the interaction of inner shell electrons with the projectiles at different projectile energies.

Vigilante et al. [21] have pointed out that binding correction plays an important role on the cross-section values. The binding correction is intrinsically a position dependent one, while in the ECPSSR theory; it is evaluated at a fixed position for each incident energy. Vigilante et al. [21] claimed that this approximation would be strictly valid only at very low incident velocities, where the impact parameter is much smaller than the radius of the shell concerned and the change in electron binding become independent of the impact parameter and may be calculated from the corresponding bindings in the United Atom (UA). They applied United Atom approximation to ECPSSR theory. The UA approximation consists in saturation of binding correction with decreasing velocity of the incident ion at the value corresponding to the binding energy of the united atom (target-projectile). They have compared the total L X-ray ionization cross-section due to proton and helium ion bombardment with the theoretical predictions due to ECPSSR and ECPSSR-UA models, and have observed that discrepancy between experimental and theoretical ECPSSR values is slightly reduced by considering UA approximation to ECPSSR theory.

Sarkadi and Mukoyama [22] pointed out that the possible reason for the discrepancies observed between experimental and theoretical predictions of L sub shell ionization cross-sections may be due to the fact that in all the theoretical approaches, the ionization of L sub shells may be treated independent of each other, neglecting the intra shell coupling effects. They pointed out that intra shell effects play an important role since the electronic wave functions of different L sub shells are close to each other. Secondary intra shell transitions may be induced between the sub shells by the projectile in the same collision, which results in a redistribution of vacancies created during the primary ionization. This vacancy sharing probability is a strong function of the atomic number of projectile and it is small for light ions. The mechanism of vacancy sharing was studied by Sarkadi and Mukoyama [22,23] in a two-step model in which the creation and rearrangement of vacancies may be treated independently. The effect of collision-induced intra shell transitions is included in the ECPSSR theory in the form of a correction factor. The same authors [24,25] developed more refined models on the basis of second order Born approximation and the simplified coupled state model [26–29]. Sarkadi and Mukoyama [26–29] have developed "coupled sub shell model" (CSM) in which they calculated the relative change of ionization caused by sub shell coupling effects assuming the dominance of the transitions to the continuum with a minimum energy transfer. Full semi-classical calculation based on 'coupled states approximation' was reported by Amundsen and Jakubassa-Amundsen [30] using target hydrogenic Dirac wave functions. A more refined coupled-channels calculations, accounting for the screening effect of the spectator electrons upon the coupling strength have been performed by Legrand et al. [31]. The inclusion of IS concept in ECPSSR theory slightly reduce the deviation between experimental L_2 ionization cross-sections and ECPSSR predictions while the deviation of L_3 cross-sections increases.

In view of the above facts, we thought it worthwhile to measure the L X-ray intensity ratios in some elements using protons with different energies, to add to the existing experimental data and also to see which theory predicts the experimental values more accurately. In the present work, the L X-ray intensity ratios are measured in the elements Hf, Ta, Re, Ir, Pt, Au and Pb with proton bombardment at projectile energies ranging from 1–5 MeV.

2 Experimental details

The present experiments are carried out at the Institute of Physics, Bhubaneswar, using 3 MV pelletron accelerator facility. Protons of different energies are employed to excite the targets, prepared by vacuum evaporation technique on to an aluminized mylar backing. The thicknesses of different targets used in the present work are ranged from 10 to 20 $\mu g/cm^2$. The targets are kept at an angle of 45° to the beam direction. The L X-ray spectra of different targets are recorded with a high resolution Si(Li) detector kept at an angle of 90° to the beam direction. The resolution of the detector is 160 eV (FWHM) at 5.9 keV energy. The spectra are collected for sufficiently long time so as to get good statistical accuracy. The L X-ray spectra are recorded for the elements Hf, Ta, Re, Ir, Pt, Au and Pb at proton energies ranging from 1–5 MeV with an interval of 1 MeV. A typical L X-ray spectrum obtained for Au at 2 MeV proton energy is shown in Figure 1.

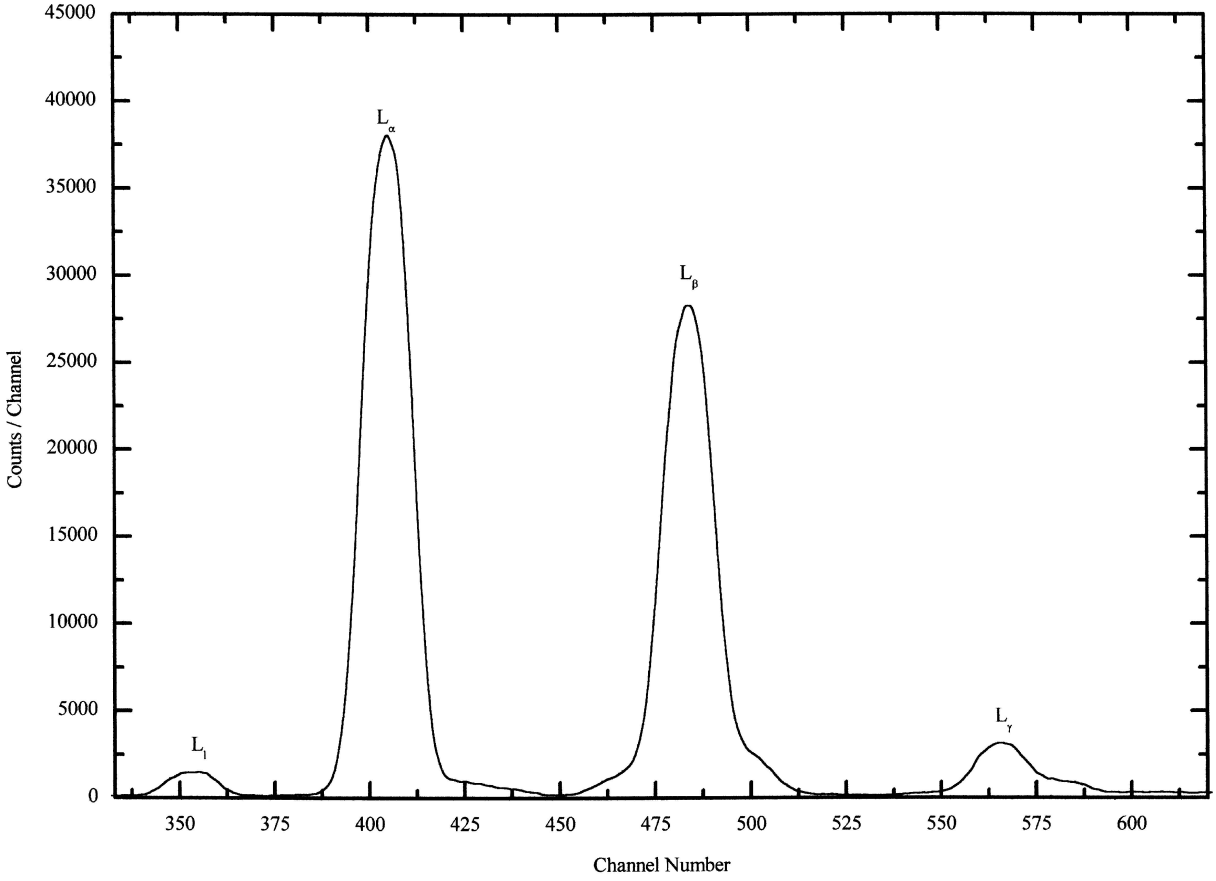

Fig. 1. The L X-ray spectrum of Pb with 2 MeV protons.

3 Data analysis

The L X-ray components L_l, L_α, L_β, and L_γ are clearly resolved for all the targets under study. The areas under different L X-ray components are carefully evaluated by using the 'Peak fit' software package. This package facilitates to define hidden peaks, which are far less apparent in the data stream by residual method. This program also facilitates the deconvolution of several unresolved peaks, which is normally done with discrete data in the Fourier domain. Peak fit also offers effective smoothing algorithms in which the local perturbations within the data are removed. This software uses an enhanced version of Levenburg-Marquardt non-linear minimization algorithms for peak fitting. For background fitting, there are several options and the option for minimum chi-square is selected. The intensities under different L X-ray components are evaluated from the areas under L X-ray components by using the efficiency values corresponding to the energies of the respective X-ray components. These intensities are corrected for self-absorption of the X-rays in the target material. The corresponding mass attenuation coefficients are taken from the tables of Storm and Israel [32]. Finally, the intensity ratios L_α/L_l, L_α/L_β and L_β/L_γ are evaluated for each element at different projectile energies. The intensity ratios L_α/L_l, L_α/L_β and L_β/L_γ thus obtained in the present work are given in Tables 1, 2 and 3 respectively.

4 Calculation of theoretical L X-ray intensity ratios

The intensity ratios of different L X-ray components is same as the ratio of the production cross-sections of the same L X-ray components. Hence, the theoretical intensity ratios L_α/L_l, L_α/L_β and L_β/L_γ are estimated by taking the theoretical production cross-section ratios of the same components. The theoretical L X-ray productions cross-sections are estimated using the theoretical ECPSSR ionization cross-sections tabulated by Cohen and Harrigan [33]. The production cross-sections are estimated using the following relations [34]

$$\sigma^X_{Ll} = (\sigma_{L1}f_{13} + \sigma_{L1}f_{12}f_{23} + \sigma_{L2}f_{23} + \sigma_{L3})\omega_3 F_{3l}$$
$$\sigma^X_{L\alpha} = (\sigma_{L1}f_{13} + \sigma_{L1}f_{12}f_{23} + \sigma_{L2}f_{23} + \sigma_{L3})\omega_3 F_{3\alpha}$$
$$\sigma^X_{L\beta} = \sigma_{L1}\omega_1 F_{1\beta} + (\sigma_{L1}f_{12} + \sigma_{L2})\omega_2 F_{2\beta} + (\sigma_{L1}f_{13} + \sigma_{L1}f_{12}f_{23} + \sigma_{L2}f_{23} + \sigma_{L3})\omega_3 F_{3\beta}$$
$$\sigma^X_{L\gamma} = \sigma_{L1}\omega_1 F_{1\gamma} + (\sigma_{L1}f_{12} + \sigma_{L2})\omega_2 F_{2\gamma}$$

where σ^X_{Ll}, $\sigma^X_{L\alpha}$, $\sigma^X_{L\beta}$ and $\sigma^X_{L\gamma}$ are the X-ray production cross-sections of L_l, L_α, L_β, and L_γ X-ray components

Table 1. The L_α/L_l intensity ratios for different elements due to proton bombardment.

Energy	Hf	Ta	Re	Ir	Pt	Au	Pb
1 MeV	21.4(P)	21.2(P)	20.8(P)	20.4(P)	20.2(P)	19.5(P)	18.2(P)
	21.9(T_1)	21.6(T_1)	21.0(T_1)	20.5(T_1)	20.2(T_1)	19.8(T_1)	18.9(T_1)
	21.9(T_2)	21.6(T_2)	21.1(T_2)	20.5(T_2)	20.2(T_2)	19.9(T_2)	18.9(T_3)
	21.96(T_3)	21.67(T_3)	21.08(T_3)	20.47(T_3)	20.18(T_3)	19.88(T_3)	18.97(T_3)
						20.06[40]	18.9[40]
						20.3[45]	18.5[41]
						17.4[47]	18.8[42]
							18.6[43]
2 MeV	21.3(P)	20.9(P)	20.5(P)	20.2(P)	20.0(P)	19.8(P)	18.7(P)
	21.9(T_1)	21.6(T_1)	21.0(T_1)	20.5(T_1)	20.2(T_1)	19.8(T_1)	18.9(T_1)
	21.9(T_2)	21.6(T_2)	21.1(T_2)	20.5(T_2)	20.2(T_2)	19.9(T_2)	18.9(T_2)
		21.5[38]		20.47(T_3)	20.18(T_3)	19.88(T_3)	18.97(T_3)
					18.7[38]	20.3[45]	20.4[41]
						18.4[47]	18.9[42]
							19.2[43]
3 MeV	21.4(P)	21.2(P)	20.6(P)	20.0(P)	20.18(P)	20.1(P)	19.2(P)
	21.9(T)	21.6(T_1)	21.0(T_1)	20.5(T_1)	20.2(T)	19.8(T_1)	18.9(T_1)
		21.6(T_2)	21.1(T_2)	20.5(T_2)	18.36[38]	19.9(T_2)	18.9(T_2)
		20.1[38]				20.3[45]	18.4[41]
							20.0[42]
							19.3[43]
4 MeV	21.4(P)	20.9(P)	20.9(P)	20.3(P)	20.4(P)	19.7(P)	19.2(P)
	21.9(T)	21.6(T_1)	21.0(T_1)	20.5(T_1)	20.2(T)	19.8(T_1)	18.9(T_1)
		21.6(T_2)	21.1(T_2)	20.5(T_2)		19.9(T_2)	18.9(T_2)
						20.3[45]	18.99[42]
						19.95[47]	19.9[48]
5 MeV	21.2(P)	21.0(P)	20.4(P)	20.2(P)	20.5(P)	19.8(P)	18.9(P)
	21.9(T)	21.6(T_1)	21.0(T_1)	20.5(T_1)	20.2(T)	19.8(T_1)	18.9(T_1)
		21.6(T_2)	21.1(T_2)	20.5(T_2)		19.9(T_2)	18.9(T_2)
						20.3[45]	19.71[42]

T_1: ECPSSR, T_2: ECPSSR-UA, T_3: ECPSSR-IS.

respectively, σ_{L1}, σ_{L2}, and σ_{L3} are the ionization cross-sections of L_1, L_2 and L_3 sub-shells respectively. ω_1, ω_2 and ω_3 are the corresponding sub-shell fluorescence yields and f_{12}, f_{23} and f_{13} are the Coster-Kronig transition probabilities.

Here F_{ny} represents τ_{ny}/τ_n. For example $F_{3\alpha} = \tau_{3\alpha}/\tau_3$ where τ_3 is the theoretical total radiative transition rate of the L_3 shell and $\tau_{3\alpha}$ is the sum of the radiative transition rates which contribute to the L_α lines associated with the hole filling in the L_3 sub-shell: that is, $\tau_{3\alpha} = \tau_3(M_4 \rightarrow L_3) + \tau_3(M_5 \rightarrow L_3)$ where $\tau_3(M_4 \rightarrow L_3)$ is the radiative transition rate from the M_4 shell to the L_3 sub shell. The radiative transition rates are taken from Scofield [35] and fluorescence yield and C-K decay yield data are taken from Krause [36] The theoretical intensity ratios of different L X-ray components thus obtained for different elements at different proton energies are also given in the Tables 1, 2 and 3 respectively.

The United Atom approximation is considered and the theoretical L X-ray intensity ratios due to ECPSSR-UA are also estimated at all energies and are given in the same tables. Similarly, considering the Intra Shell coupling effects, the theoretical L X-ray intensity ratios due to ECPSSR-IS are also calculated. However, it is not possible to estimate ECPSSR-IS theoretical ratios at all proton energies. This is because the multiplication factors due to IS effect to the ECPSSR values are furnished by Sarkadi and Mukoyama [37] only within the limits of reduced velocities below 0.8. This condition is satisfied for elements Hf, Ta and Re for proton energies of 1 MeV, and for Ir, Pt, Au and Pb for proton energies of 1 and 2 MeV energies. Hence, only for these energies, the theoretical intensity ratios due to ECPSSR-IS predictions are calculated and furnished in the same tables.

5 Results and discussion

From the areas under individual X-ray components, the relative intensities L_α/L_l, L_α/L_β and L_β/L_γ are estimated. Since only the relative intensities and not absolute intensities are measured, the uncertainties in inhomogeneity of target, uncertainties in geometric parameters such as solid angle of the detectors, uncertainty in Rutherford backscattering cross-sections get eliminated. Thus the only uncertainties to be considered are those in counting statistics and in detector efficiency values. Hence, the present experimental intensity ratios are associated with an overall uncertainty of 3%, arising by 2% uncertainty in counting statistics, and 2% uncertainty in efficiency values.

Table 2. The L_α/L_β intensity ratios for different elements due to proton bombardment.

Energy	Hf	Ta	Re	Ir	Pt	Au	Pb
1 MeV	1.71(P)	1.9(P)	1.84(P)	1.87(P)	1.97(P)	1.88(P)	1.75(P)
	2.0(T_1)	2.0(T_1)	1.93(T_1)	2.1(T_1)	2.2(T_1)	2.2(T_1)	2.2(T_1)
	2.0(T_2)	2.03(T_2)	2.07(T_2)	2.13(T_2)	2.15(T_2)	2.17(T_2)	2.22(T_2)
	2.02(T_3)	2.02(T_3)	2.09(T_3)	2.07(T_3)	2.08(T_3)	2.09(T_3)	2.10(T_3)
		1.82[39]			1.88[46]	1.86[40]	1.90[40]
						1.78[44]	1.84[41]
						1.89[47]	2.06[42]
						1.78[45]	1.86[43]
						1.89[50]	1.76[46]
2 MeV	1.52(P)	1.7(P)	1.72(P)	1.68(P)	1.83(P)	1.78	1.69
	1.76(T_1)	1.8(T_1)	1.84(T_1)	1.93(T_1)	2.00(T_1)	2.00(T_1)	2.1(T_1)
	1.76(T_2)	1.78(T_2)	1.85(T_2)	1.94(T_2)	1.97(T_2)	2.00(T_2)	2.08(T_2)
				1.97(T_3)	2.00(T_3)	2.002(T_3)	2.07(T_3)
					1.80[38]	1.61[44]	1.73[41]
					1.67[46]	1.77[47]	1.84[42]
						1.65[46]	1.73[43]
						1.75[19]	
						1.76[51]	
3 MeV	1.43(P)	1.4(P)	1.67(P)	1.61(P)	1.68(P)	1.69(P)	1.64(P)
	1.6(T_1)	1.6(T_1)	1.74(T_1)	1.76(T_1)	1.80(T_1)	1.83(T_1)	1.9(T_1)
	1.55(T_2)	1.57(T_2)	1.64(T_2)	1.76(T_2)	1.80(T_2)	1.84(T_2)	1.91(T_2)
					1.63[38]	1.57[46]	1.66[41]
					1.54[46]	1.63[45]	1.7[42]
						1.65[47]	1.62[43]
						1.56[46]	1.75[50]
						1.67[50]	
						1.68[19]	
						1.64[51]	
4 MeV	1.4(P)	1.38(P)	1.54(P)	1.55(P)	1.58(P)	1.46(P)	1.58(P)
	1.44(T_1)	1.45(T_1)	1.62(T_1)	1.64(T_1)	1.70(T_1)	1.73(T_1)	1.80(T_1)
	1.44(T_2)	1.45(T_2)	1.52(T_2)	1.65(T_2)	1.69(T_2)	1.73(T_2)	1.80(T_2)
						1.51[44]	1.67[42]
						1.6[47]	1.55[48]
							1.59[49]
5 MeV	1.33(P)	1.33(P)	1.37(P)	1.42(P)	1.54(P)	1.39(P)	1.48(P)
	1.38(T_1)	1.38(T_1)	1.45(T_1)	1.58(T_1)	1.62(T_1)	1.66(T_1)	1.73(T_1)
	1.38(T_2)	1.38(T_2)	1.45(T_2)	1.58(T_2)	1.63(T_2)	1.67(T_2)	1.73(T_2)
						1.47[44]	1.62[42]
							1.56[49]

T_1: ECPSSR, T_2: ECPSSR-UA, T_3: ECPSSR-IS.

5.1 L_α/L_l intensity ratios

The L_l and L_α X-ray components arise due to the filling of L_3 sub shell vacancies. The L_l line arises due to $M_1 \rightarrow L_3$ transition. The L_α component is the sum of $L_{\alpha 1}$ and $L_{\alpha 2}$ lines, which arise due to $M_5 \rightarrow L_3$ and $M_4 \rightarrow L_3$ transitions respectively. The L_α/L_l intensity ratios for different elements at different projectile energies obtained in the present work is given in Table 1 along with the corresponding theoretical values and those reported by previous authors. The theoretical L_α/L_l intensity ratios are independent of proton energy. The present L_α/L_l intensity ratios are in good agreement with the theoretical values and the values due to other authors for all the elements within experimental uncertainties.

5.2 L_α/L_β intensity ratios

The L_β peak is the sum of several individual L_β components. Out of these components, the $L_{\beta 1}$ ($M_4 \rightarrow L_2$), $L_{\beta 2}$ ($N_5 \rightarrow L_3$), $L_{\beta 3}$ ($M_3 \rightarrow L_1$), $L_{\beta 4}$ ($M_2 \rightarrow L_1$) and $L_{\beta 5}$ ($O_{4,5} \rightarrow L_3$) are intense, while the others are relatively weak. In the present experiment, since Si(Li) detector is used, the individual L_β X-ray components do not get resolved. Hence, the total intensity under L_β line is measured. The L_α/L_β intensity ratios obtained in the present work for different elements Hf, Ta, Re, Ir, Pt, Au and Pb at different projectile energies are given in Table 2 along with the corresponding theoretical values and values reported by previous authors. Since, most of the earlier published data is available in graphical form, it is not possible to furnish previous data for all the elements under study. The present L_α/L_β intensity ratios for the

Table 3. The L_β/L_γ intensity ratios for different elements due to proton bombardment.

Energy	Hf	Ta	Re	Ir	Pt	Au	Pb
1 MeV	7.3(P)	7.2(P)	7.3(P)	7.1(P)	6.7(P)	7.2(P)	7.05(P)
	8.4(T_1)	8.3(T_1)	8.0(T_1)	8.3(T_1)	8.3(T_1)	8.4(T_1)	8.61(T_1)
	8.42(T_2)	8.37(T_2)	8.3(T_2)	8.42(T_2)	8.48(T_2)	8.5(T_2)	8.68(T_2)
	88.44(T_3)	8.37(T_3)	8.42(T_3)	8.29(T_3)	8.30(T_3)	8.27(T_3)	8.25(T_3)
					7.1[46]	7.1[44]	7.22[40]
						7.31[40]	8.12[41]
						6.9[47]	9.32[42]
						6.5[45]	6.88[43]
						7.4[50]	
2 MeV	7.0(P)	7.1(P)	7.2(P)	6.2(P)	6.7(P)	6.9(P)	6.98(P)
	7.7(T_1)	7.7(T_1)	7.8(T_1)	7.9(T_1)	8.0(T_1)	8.0(T_1)	8.1(T_1)
	7.63(T_2)	7.68(T_2)	7.75(T_2)	7.91(T_2)	7.97(T_2)	8.0(T_2)	8.15(T_2)
				7.99(T_3)	8.05(T_3)	8.10(T_3)	8.21(T_3)
					7.27[38]	6.9[51]	6.66[41]
					6.7[46]	6.6[44]	7.23[42]
						6.6[47]	6.42[43]
						7.3[45]	
						6.9[46]	
						6.95[19]	
3 MeV	6.4(P)	7.0(P)	7.0(P)	6.0(P)	6.6(P)	6.83(P)	6.8(P)
	7.1(T_1)	7.1(T_1)	7.2(T_1)	7.4(T_1)	7.4(T_1)	7.5(T_1)	7.6(T_1)
	7.07(T_2)	7.08(T_2)	7.12(T_2)	7.34(T_2)	7.42(T_2)	7.5(T_2)	7.61(T_2)
					7.15[38]	6.11[44]	6.36[41]
					6.4[46]	6.25[45]	7.15[42]
						6.25[47]	5.96[43]
						6.71[46]	5.71[50]
						6.88[50]	
						6.69[19]	
						6.3[51]	
4 MeV	5.7(P)	6.6(P)	6.3(P)	5.8(P)	6.55(P)	6.80(P)	6.7(P)
	6.8(T_1)	6.7(T_1)	6.8(T_1)	7.02(T_1)	7.11(T_1)	7.2(T_1)	7.3(T_1)
	6.79(T_2)	6.76(T_2)	6.79(T_2)	7.02(T_2)	7.1(T_2)	7.2(T_2)	7.26(T_2)
						5.8[44]	6.62[42]
						6.01[47]	6.44[48]
							6.92[49]
5 MeV	4.7(P)	6.6(P)	6.0(P)	5.7(P)	6.4(P)	6.7(P)	6.5(P)
	6.6(T_1)	6.5(T_1)	6.61(T_1)	6.83(T_1)	6.9(T_1)	7.0(T_1)	7.1(T_1)
	6.64(T_2)	6.6(T_2)	6.61(T_2)	6.83(T_2)	6.9(T_2)	6.98(T_2)	7.1(T_2)
						5.6[44]	6.7[42]
							6.89[49]

T_1: ECPSSR, T_2: ECPSSR-UA, T_3: ECPSSR-IS.

elements are plotted against projectile energies and are shown in Figure 2.

For tantalum, the L_α/L_β ratio reported by Jesus et al. at 1 MeV proton energy is slightly lower than the present value, while for the element Pt, the present value is slightly higher than the value reported by Khan et al. [46] at proton energies 1, 2 and 3 MeV and is in agreement with those reported by Braziewicz et al. [38] at 2 and 3 MeV. For the element Au, the present L_α/L_β values are in agreement with those due to Jesus et al. [40] at 1 MeV energy, Tawara et al. [47] at 1, 2 and 3 MeV, with Close et al. [50] at 1 and 3 MeV, with Campbell [19] at 2 and 3 MeV energies. For the same element, the present values are higher than those due to Sokhi and Crumpton [45] and Shafroth et al. [44] at proton energies 1, 2 and 3 MeV. In Pb element also, the present L_α/L_β are in good agreement with some of the earlier authors within experimental uncertainties.

From Figure 2 and Table 2, it is seen that the present L_α/L_β intensity ratios are lower than the theoretical values due to ECPSSR and ECPSSR-UA predictions for all the elements under study at all projectile energies. Also, from Table 2, it is seen that the same intensity ratios reported by other earlier authors are also lower than the theoretical values for all elements at all projectile energies.

5.3 L_β/L_γ intensity ratios

The L_β/L_γ intensity ratios obtained in the present work for the elements under study at different proton energies

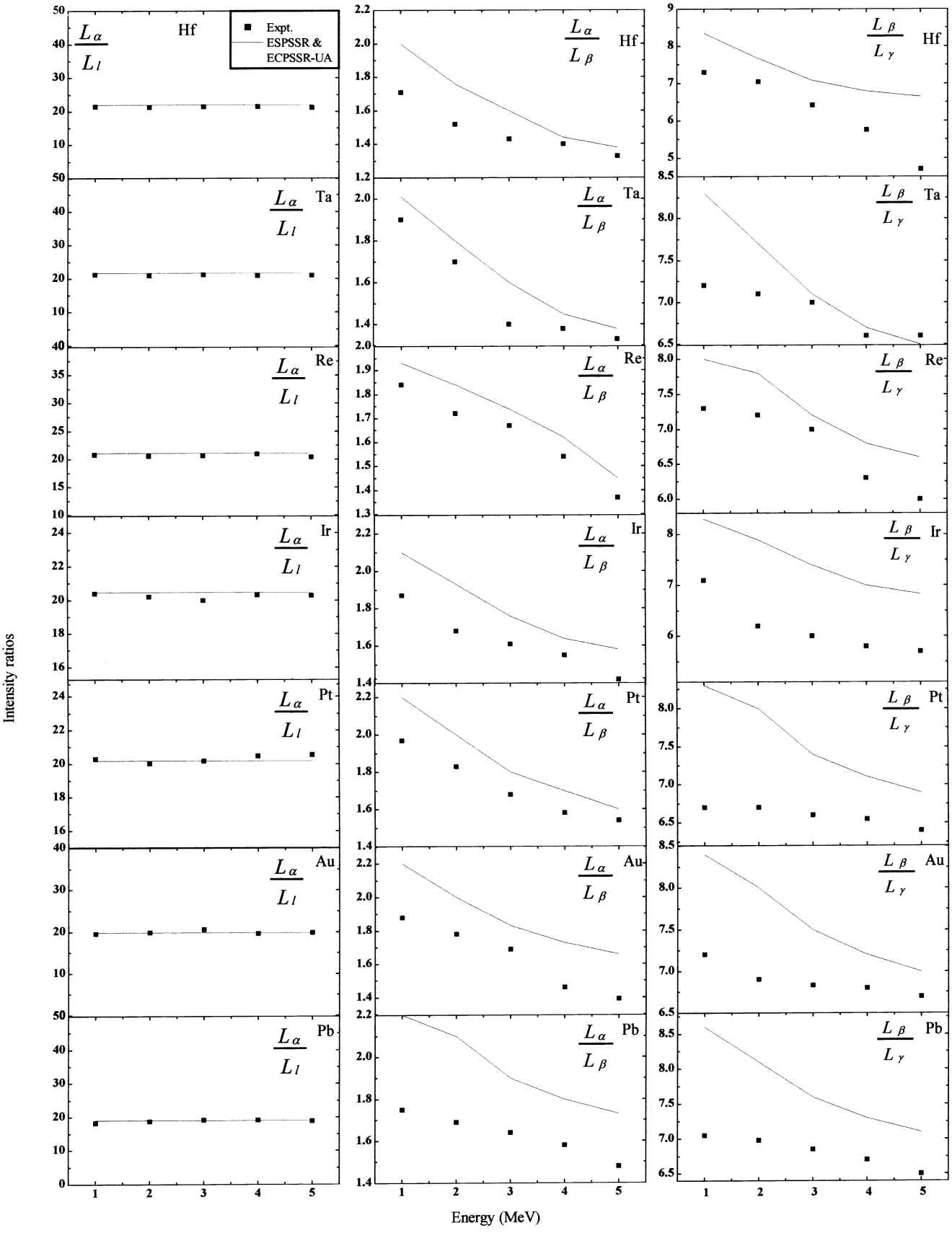

Fig. 2. L X-ray intensity ratios in different elements at proton energies 1–5 MeV.

are given in Table 3 along with the corresponding theoretical values and the values reported by previous authors. The L_β/L_γ intensity ratios obtained in the present experiment are plotted against projectile energies and are shown in Figure 2. The present L_β/L_γ intensity ratios are in good agreement with the data reported by many of the earlier authors within experimental uncertainties. However, as seen from Figure 2 and from Table 3, it is evident that the present L_β/L_γ intensity ratios and many of the values reported by earlier authors are systematically lower than the theoretical intensity ratios for all the elements under study at all projectile energies. The deviation decreases as projectile energy increases.

6 Possible multiple ionization effects

In the present work, the experimental intensity ratios L_α/L_β and L_β/L_γ are lower than theoretical ECPSSR and ECPSSR-UA predictions, particularly at low energies. This deviation may be explained in terms of possible multiple ionization effects.

In charged particle collision, multiple ionization effects are predominant, which can be observed by changes in the X-ray energies and intensity ratios of different X-ray components. In K shell ionization process, simultaneous vacancies produced in L shell alter the screening of nuclear charge felt by the transition electrons from M, N, O... shells. This results in an increase in the K X-ray energies and K_β/K_α intensity ratios. Such energy shifts in K X-ray components and increase in K_β/K_α intensity ratios are observed by Li et al. [52] and Ramachandra Rao et al. [53]. Similarly, such energy shifts in different L X-ray components are observed by Szokefalvi-Nagy et al. [43]. Here it is remarked that the multiple ionization effects are to be observed only in the intensity ratios of those X-ray components for which the final state of the transition electrons is the same.

The observation of multiple ionization effects during L shell ionization process is possible from the following intensity ratios

$$[L_{\beta1}(M_4 \rightarrow L_2)] \text{ to } [L_{\gamma1}(N_4 \rightarrow L_2) + L_{\gamma5}(N_1 \rightarrow L_2) + L_{\gamma6}(O_4 \rightarrow L_2) + L_{\gamma8}(O_1 \rightarrow L_2)] \quad (1)$$

$$[L_{\beta4}(M_2 \rightarrow L_1) + L_{\beta3}(M_3 \rightarrow L_1) + L_{\beta9,10}(M_{4,5} \rightarrow L_1)] \text{ to } [L_{\gamma2}(N_2 \rightarrow L_1) + L_{\gamma3}(N_3 \rightarrow L_1) + L_{\gamma11}(N_5, O_2 \rightarrow L_1)] \quad (2)$$

$$[L_{\alpha2}(M_4 \rightarrow L_3) + L_{\alpha1}(M_5 \rightarrow L_3)] \text{ to } [L_{\beta2}(N_5 \rightarrow L_3) + L_{\beta5}(O_{4,5} \rightarrow L_3) + L_{\beta6}(N_1 \rightarrow L_3) + L_{\beta7}(O_1 \rightarrow L_3) + L_{\beta15}(N_5 \rightarrow L_3)]. \quad (3)$$

In the present work, since Si(Li) detector is employed for X-ray measurement, owing to its poor resolution, the L_β and L_γ X-ray components are not resolved. Hence, to observe multiple ionization effects we could only consider the total intensity ratios of L_β/L_γ and L_α/L_β instead of $L_{\beta1}/L_{\gamma1,5,6,8}$ and $L_\alpha/L_{\beta2,5,6,7,15}$ respectively. This is justified since in both cases, the change in relative intensities of the components due to multiple ionization will be reflected in the total intensity ratios also as the relative intensities of the components are of appreciable magnitude. Between these two sets of relative intensities, the relative magnitude of $L_{\beta1}/L_{\gamma1,5,6,8}$ with respect to L_β/L_γ is much larger when compared to the relative magnitude of $L_\alpha/L_{\beta2,5,6,7,15}$ with respect to L_α/L_β and hence the changes in relative intensity due to multiple ionization are reflected more strongly in the former ratio.

If there is considerable multiple ionization with simultaneous vacancies in M shell, the transition rates of $L_{\beta1}$ X-ray component decreases while the transition rates of $L_{\gamma1,5,6,8}$ increases. Hence, the ratio $L_{\beta1}/L_{\gamma1,5,6,8}$ decreases compared with that due to normally excited atoms. Similarly, the transition rates of the L X-ray components (L_α) arising due to the transfer of electrons from M shell to L shell also decrease while the transition rates of the L X-ray components ($L_{\beta2,5,6,7,15}$) arising due to the transfer of electrons from N and O to L shell increase. As a result, the intensity ratios $L_\alpha/L_{\beta2,5,6,7,15}$ decrease compared with the same ratios in the absence of multiple ionization.

In the present work, the experimental L_β/L_γ and L_α/L_β intensity ratios are compared with ECPSSR and ECPSSR-UA theoretical predictions. The theoretical intensity ratios of different L X-ray components are same as the ratios of the corresponding production cross-sections. The theoretical production cross-sections are evaluated from the theoretical ionization cross-sections employing different atomic parameters corresponding to single hole values without considering the effect of multiple ionization.

From a comparison of the present L_β/L_γ and L_α/L_β intensity ratios with theoretical ECPSSR predictions, it is observed that at low projectile energies, the experimental intensity ratios are lower than the theoretical values. This discrepancy may be attributed to multiple ionization effects, which are not taken into consideration in the theory. The small difference between experimental and theoretical intensity ratios may be due to low multiply ionization effects caused by proton bombardment. As the projectile energy increases, the deviation between theory and experiment gradually decreases. This trend may be explained in terms of the lowering of multiple ionization with increase in projectile energy as the deviation is caused by multiple ionization.

7 Conclusions

The L_α/L_l, L_β/L_γ and L_α/L_β intensity ratios are measured in the elements Hf, Ta, Re, Ir, Pt, Au and Pb at proton energies from 1 to 5 MeV. The experimental intensity ratios are compared with the theoretical intensity ratios calculated by using ECPSSR and ECPSSR-UA ionization cross-sections. These intensity ratios are in agreement with the values due to earlier authors. The present L_α/L_l intensity ratios are in good agreement with theoretical values while the present L_β/L_γ and L_α/L_β intensity

ratios are consistently lower than the theoretical values. This deviation may be attributed to multiple ionization effects in M, N and O shells.

One of the authors Dr. S. Bhuloka Reddy gratefully acknowledges the financial support provided by the Inter University Consortium for DAE facilities, Kolkata Centre, India. The authors express their sincere thanks to the authorities of the Institute of Physics, Bhubaneswar, for providing accelerator facility.

References

1. H.A. Bethe, Ann. Phys. (Leipzig) **5**, 325 (1930)
2. E. Merzbacher, H.W. Lewis, *Handbuch der Physik*, edited by S. Flugge (Springer, Berlin, 1958), Vol. 24, p. 166
3. B.H. Choi, E. Merzbacher, G.S. Khandelwal, At. Data **5**, 291 (1973)
4. J. Bang, J.M. Hansteen, K. Dan, Vidensk Selsk. Mat. Fys. Med. **31**, 13 (1959)
5. J.M. Hansteen, O.P. Mosebekk, Z. Phys. **234**, 281 (1971)
6. M. Gryzinski, Phys. Rev. **138**, A238 (1965); Phys. Rev. **138**, A304 (1965); Phys. Rev. **138**, A322 (1965)
7. W. Brandt, G. Lapicki, Phys. Rev. A **20**, 465 (1979)
8. W. Brandt, G. Lapicki, Phys. Rev. A **23**, 1717 (1981)
9. H. Paul, J. Sacher, At. Data Nucl. Data Tables **42**, 105 (1989)
10. H. Paul, O. Bolik, At. Data Nucl. Data Tables **54**, 75 (1993)
11. R.S. Sokhi, D. Crumpton, At Data Nucl. Data tables **30**, 49 (1984)
12. I. Orlic, C.H. Sow, S.M. Tang, At Data Nucl Data tables **56**, 159 (1994)
13. W. Jitschin, A. Kaschaba, R. Hippler, H.O. Lutz, J. Phys. B **15**, 763 (1982)
14. J. Braziewicz, M. Pajek, E. Braziewicz, J. Ploskonka, J. Phys. B **17**, 3245 (1984)
15. J. Braziewicz, M. Pajck, E. Braziewiczand, J. Ploskonka, G.M. Osetynski, Nucl. Instrum. Meth. B **15**, 585 (1980)
16. M. Vigilante, P. Cuzzocrea, N. Decesare, F. Muroloilante, M. Cuzzocrea, P. Decesare, N. Murolo, F. Perillo, E. Spadaccimi, Nucl. Instrum. Meth. B **15**, 576 (1986)
17. T.J. Gray, N. Malhi, Bull. Am. Phys. Soc. **35**, 1713 (1990)
18. M. Harrigan, D.D. Cohen, Nucl. Instrum. Meth. B **31**, 576 (1986)
19. J.L. Campbell, Nucl. Instrum. Meth. B **31**, 518 (1988)
20. G. Lapicki, Nucl. Instrum. Meth. B **189**, 8 (2002)
21. M. Vigilante, P. Cuzzocrea, N. De Cesare, F. Murolo, E. Perillo, G. Spadaccini, Nucl. Instrum. Meth. B **51**, 232 (1990)
22. L. Sarkadi, T. Mukoyama, J. Phys. B **13**, 2255 (1980)
23. L. Sarkadi, T. Mukoyama, J. Phys. B **14**, L255 (1981)
24. L. Sarkadi, T. Mukoyama, Nucl. Instrum. Meth. Phys. Res. B **4**, 296 (1984)
25. L. Sarkadi, J. Phys. B **19**, 2519 (1986)
26. L. Sarkadi, J. Phys. B **19**, L755 (1986)
27. L. Sarkadi, T. Mukoyama, J. Phys. B **20**, L559 (1987)
28. L. Sarkadi, T. Mukoyama, J. Phys. B **23**, 3849 (1990)
29. L. Sarkadi, T. Mukoyama, Z. Smit, J. Phys. B **29**, 2253 (1996)
30. P.A. Amundsen, D.H. Jakubassa-Amundsen, J. Phys. B **21**, L99 (1988)
31. I.C. Legrand, V. Zoran, R. Dorner, H. Schmidt-Bocking, A. Berinde, D. Fluerasu, C. Ciortea, J. Phys. B **25**, 189 (1992)
32. E. Storm, H.J. Israel, Nucl. Data Tables A **7**, 565 (1970)
33. M. Cohen, D.D. Harrigan, At. Nucl. Data. Tables **33**, 255 (1985)
34. H.C. Padhi, C.R. Buniya, B.B. Dhal, S. Misra, J. Phys. B **27**, 1105 (1994)
35. J.H. Scofield, At. Data. Nucl. Data. Tables **14**, 121 (1974)
36. M.O. Krause, J. Phys. Chem. Ref. Data **8**, 307 (1979)
37. L. Sarkadi, T. Mukoyama, Nucl. Instrum. Meth. Phys. Res. B **61**, 167 (1991)
38. J. Braziewicz, M. Pajek, E. Braziewicz, J. Ploskonka, G.M. Osetynski, J. Phys. B **17**, 1589 (1984)
39. A.P. Jesus, J.P. Ribeiro, J.S. Lopes, J. Phys. B **20**, 95 (1987)
40. A.P. Jesus, J.S. Lopes, J.P. Ribeiro, J. Phys. B **18**, 2453 (1985)
41. R.S. Sokhi, D. Crumpton, Nucl. Instrum. Meth. **192**, 121 (1982)
42. C.E. Busch, A.B. Baskin, P.H. Nettles, S.M. Shafroth, A.W. Waltner, Phys. Rev. A **7**, 1601 (1973)
43. Z. Szokefalvi-Nagy, I. Demeter, L.H. Quynh, Nucl. Instrum. Meth. B **75**, 54 (1993)
44. S.M. Shafroth, G.A. Bissinger, A.W. Waltner, Phys. Rev. A **7**, 566 (1973)
45. R.S. Sokhi, D. Crumpton, Nucl. Instrum. Meth. **181**, 5 (1981)
46. M.R. Khan, A.G. Hopkins, D. Crumpton, Z. Phys. A **288**, 133 (1978)
47. H. Tawara, K. Ishii, S. Morita, H. Kaji, T. Shiokawa, Phys. Rev. A **111**, 560 (1975)
48. H. Tawara, K. Ishii, S. Morita, H. Kaji, C.N. Hsu, T. Shiokawa, Phys. Rev. A **9**, 1617 (1974)
49. R.B. Liebert, T. Zabel, D. Miljanic, H. Larson, V. Valkovic, C. Phillips, Phys. Rev. A **8**, 2336 (1973)
50. D.A. Close, R.C. Bearse, J.J. Malanify, C.J. Umbarger, Phys. Rev. A **8**, 1873 (1973)
51. M.H Chen, B. Crasemann, H. Mark, Phys. Rev. A **24**, 177 (1981)
52. T.K. Li, R.L. Watson, Phys. Rev. A **9**, 1574 (1974)
53. K.R. Rao, Y.R. Krishna, P. Venkateswarlu, K.B. Rao, V.S. Rao, G.J.N. Raju, S.B. Reddy, Eur. Phys. J. D **15**, 283 (2001)